KEMENTERIAN SUMBER ASLI, ALAM SEKITAR
DAN PERUBAHAN IKLIM
Ministry of Natural Resources, Environment
and Climate Change

MALAYSIAN METEOROLOGICAL DEPARTMENT
MINISTRY OF NATURAL RESOURCES, ENVIRONMENT
AND CLIMATE CHANGE

# Technical Note No. 2/2023

## Fine Tuning an NWP Blended Radar Nowcasting System During Two Severe Rainstorm Events

Yip Weng Sang, Diong Jeong Yik,
Nursalleh K. Chang @ bin Kassim,
Muhammad Firdaus Ammar bin Abdullah,
Fadila Jasmin binti Fakaruddin,
Woo Wang Chun and Wong Wai Kin

TECHNICAL NOTE NO. 2/2023

# Fine Tuning an NWP Blended Radar Nowcasting System During Two Severe Rainstorm Events

By
Yip Weng Sang, Diong Jeong Yik,
Nursalleh K. Chang @ bin Kassim,
Muhammad Firdaus Ammar bin Abdullah,
Fadila Jasmin binti Fakaruddin, Woo Wang Chun and
Wong Wai Kin

Perpustakaan Negara Malaysia Data Pengkatalogan-dalam-Penerbitan

Cataloguing-in-Publication Data

Perpustakaan Negara Malaysia

A catalogue record for this book is available from the National Library of Malaysia

ISBN 978-967-2327-17-2

**Published and printed by:**
Jabatan Meteorologi Malaysia
Jalan Sultan
46667 Petaling Jaya
Selangor Darul Ehsan
Malaysia

# Contents

# Fine Tuning an NWP Blended Radar Nowcasting System During Two Severe Rainstorm Events

Yip Weng Sang[1], Diong Jeong Yik, Nursalleh K. Chang @ bin Kassim, Muhammad Firdaus Ammar bin Abdullah, Fadila Jasmin binti Fakaruddin, Woo Wang Chun[3], Wong Wai Kin[2]

1 Malaysian Meteorological Department, Malaysia
2 Hong Kong Observatory, Hong Kong, China
3 Unaffiliated, Bristol, United Kingdom
Email: [1]yipws@met.gov.my, [2]wkwong@hko.gov.hk, [3]solowoo@icloud.com

## Abstract

The Radar Integrated Nowcasting System (RaINS) has been developed and put into operation in the Malaysian Meteorological Department (MMD) as a new nowcasting system that generates rainfall prediction up to 3 hours ahead. RaINS seamlessly combines radar-based extrapolation nowcast with forecast of convection-permitting numerical weather prediction (NWP) model in MMD. It is based on the blending algorithm adopted in the SWIRLS ("Short-range Warning of Intense Rainstorms in Localized Systems") nowcasting system of the Hong Kong Observatory (HKO). To determine the most suitable prognostic output of NWP in blending with SWIRLS nowcast, the model-simulated maximum reflectivity from 1000hPa to 100hPa along with the simulated average reflectivity fields from 850-750hPa and 850-500hPa were examined in this study. Using CAPPI at 2km of height as verifying observation, the performance of RaINS was verified using two significant cyclone cases in Peninsular Malaysia. It was found that blending with maximum reflectivity was more accurate than using the averaged reflectivity fields. Additionally, a higher skill score was obtained when the radar motion vector was computed using ensemble average motion vector as opposed to using single member motion vector. Then forecasting skill can be improved with persistence in the hyperbolic tangent function used to blend SWIRLS output with NWP forecast. Future direction of the development of RaINS such as using deep learning precipitation nowcasting for radar extrapolation together with assimilation of near real time observation data into NWP model are discussed.

## 1. Introduction

Nowcasting and very short-range forecasting techniques are based on detailed description of the present weather. The period of nowcast is usually up to 6 hours after the initial observation time. This is a critical time window for flash flood and landslide risk assessments, especially over densely populated urban areas, and complex terrain. In the Malaysian Meteorological Department (MMD), radar data are used in nowcasting because they can detect precipitation over a long range of up to 300km at a fine resolution of 1km and at frequent intervals of once every 10 minutes. Over the past decades, diverse nowcast techniques have been developed to extrapolate observed radar echoes into the near future to predict short-term rainfall intensity and distribution.

Operational nowcasting methods can be classified generally into three approaches, namely the object-based method, the pixel-based method, and NWP models. The object-based approach identifies the storm centroid in one radar image and calculates the speed of that centroid based on its position in the next image. Object-based methods include SCIT (Storm Cell Identification and Tracking algorithm) [1], TITAN (Thunderstorm Identification, Tracking, Analysis, and Nowcasting) [2], and TRT (Thunderstorms Radar Tracking) [3]. Since a single velocity vector is associated with a centroid, this method may be deficient if the shape of the storm edge changes between consecutive radar images [1]. Object-based methods may not detect storm cells of all shapes, sizes, and intensity because storms are rigidly classified as areas of consecutive reflectivity within a range of reflectivity intensities [1–3]. Object-based methods simplify the domain into a few storm cells; therefore, it is more sensitive to error propagation from errors in storm cell identification, trajectory, merges, and splitting. On the other hand, the pixel-based method calculates gridded motion vectors at each pixel as a dense motion field over the domain. This suggests that the pixel-based method accounts for storms of all shapes, sizes, and intensity [4]. An example of a pixel-based method is TREC (Tracking Radar Echoes by Correlation Technique) reported by [5]. TREC determines the motion vector based on maximum correlation between two consecutive radar images. [6] reported that TREC produced realistic wind fields of mesoscale weather systems. [7] adapted the TREC method for nowcasting in complex orography by imposing smoothing and continuity constraints upon TREC motion vectors. Nevertheless, both the object-based and pixel-based approaches are not able to dynamically account for radar echo growth and decay. This would lead to rapid decrease in predictive skill within the first few hours of severe weather. By far NWP models are the best because they resolve

atmospheric flow through complex terrain and capture current atmospheric conditions through assimilating near real time station, radar, and satellite observation data. However, this NWP approach requires expensive computing power compared to the pixel and object-based methods. A compromise between accuracy and computing power would be to primarily use a pixel-based approach at very short lead time and then assign more weight to NWP models to compensate for the drop in skill [8]. This is the approach utilized in the Radar Integrated Nowcasting System (RaINS) operated by the MMD.

The RaINS nowcasting system is based upon the RAPIDS (Rainstorm Analysis and Prediction Integrated Data-processing System) developed by the Hong Kong Observatory (HKO) [9,10]. The nowcast component, i.e., radar-based extrapolation in RaINS and RAP-IDS is based on SWIRLS (Short-range Warning of Intense Rainstorms in Localized Systems) that performed favourably compared to other pixel-based radar extrapolation methods [11]. The hyperbolic tangent weighting function is employed to blend SWIRLS now-cast with the corrected QPF (quantitative precipitation forecast) from the convection-permitting NWP model. The corrections applied to NWP QPF includes bias correction using the Weibull distribution to nudge NWP reflectivity values closer to observed radar values. Descriptions of bias correction methods can be referred to in [8,9]. Nevertheless, the difference between RaINS and RAPIDS lies in the hyperbolic tangent function that is utilized to blend SWIRLS output with NWP output. RaINS can be configured to use several different hyperbolic tangent weighting functions but choose only one weighting function which gives the SWIRLS-NWP blend closest to radar observations 3 hours ago. The chosen weight may vary in each nowcast cycle, as compared to a single weighting function adopted in the original [9].

The RAPIDS has been shown to be skilful in very short-term forecasts of convective storms of sub-synoptic to meso-$\boldsymbol{\alpha}$ scales [6,9,10,12,13]. Therefore, it is expected that RaINS in MMD may also be skilful for the meteorological processes of similar spatial scales in Malaysia. This is confirmed by the work of [14] who studied the skill of RaINS during a cyclonic vortex event. Therefore, this study aims to examine the robustness of the RaINS configuration by including an additional cyclonic vortex event. In this study, besides evaluating the big storm event induced by the cyclonic vortices, we also determine the skill of RaINS in forecasting convective rainfall events that took place at the same time. Using these events as assessments, this would enable us to fine-tune RaINS through testing various simulated reflectivity fields from NWP model, and to examine the usage of an optical flow average from multiple flow parameters. In addition,

the current RaINS configuration that selects one out of many hyperbolic tangent weighting functions based on past radar observations to nowcast was compared against the RaINS configuration where a constant non-variable single hyperbolic tangent weighing function was used. This was done to assess the impact of persistency upon nowcast accuracy where the selection of SWIRLS-NWP blending function was not constant but based upon the most optimal blending weight three hours ago [14].

The input radar and NWP data used in this study are described in **Section 2** and the configuration of RaINS tested in this study outlined in **Section 3**. Thereafter, the performance of RaINS at these events is discussed in **Section 4**. Consequently, the optimal configuration of RaINS to be used operationally and the way forward are proposed in **Section 5**.

## 2. Data

The input radar data of RaINS are the 2km CAPPI (Constant Altitude Plan Position Indicator) reflectivity (in dBZ), denoted by CAPPI-2km hereinafter, are obtained from the 13 operational radar stations of the MMD depicted in **Figure 1**. The spacing between grid points is 0.833 km with an update frequency of 10 minutes. [15] used CAPPI-1km for radar-based nowcasting of cyclone Ogni in India while [11] reported that the typical operational product of HKO SWIRLS used CAPPI-2km instead. [16] analysed the radar beam range with respect to topography and reported that CAPPI-1km in Malaysia is more prone to terrain blockage compared to CAPPI-2km. Additionally, visual analysis of radar images during several heavy rainfall events was performed [16], and it was reported that CAPPI-1km can be more susceptible to ground clutter. Therefore, based on [16] we conclude that CAPPI-2km is the most suitable height for sampling radar reflectivity. CAPPI-2km data was integrated to a common configuration of grid points through the inverse distance weighted interpolation method to the power of unity, whereby the maximum reflectivity value is taken if there is an overlap of more than one radar. The inclusion of all radar stations within a combined common grid reduces the risk of heavy rainfall events being un-detected, as well as to filter spurious noise in CAPPI data as input to RaINS if a single radar captures unrealistically strong reflectivity.

The Weather Research and Forecasting (WRF) model was used in this study [17]. The non-hydrostatic dynamical core is used in the MMD-WRF system, with the physical pro-cesses including the Dudhia radiation scheme, and the Thompson microphysics scheme and the YSU boundary layer parameterization scheme. Convective

parameterization scheme was disabled in MET-WRF as the horizontal resolution is 1km that should explicitly resolve the cloud microphysics at grid scale. The horizontal domain shown in **Figure 2** has a 1km resolution consisting of 771 meridional grid points, 2196 zonal grid points and 51 vertical levels. This is the innermost domain within a 3-way nesting configuration. The MET-WRF was initialized 4 times a day at 00Z, 06Z, 12Z, and 18Z by NCEP GFS fore-cast data at 0.25-degree latitude/longitude resolution. Currently there is no data assimilation applied although the MMD plans to introduce satellite data assimilation soon. Although the largest to smallest domain have forecast length of 168 hours, RaINS only in-gests the latest 6-hourly MET-WRF run, subject to at least 6 hours spin-up time. Usage of the most recent MET-WRF run avoids the forecast from being fully driven by large-scale forcing from the parent domains at longer lead time. Due to constraints in computational power, it is not possible to run MET-WRF in Rapid Update Cycle (RUC) configuration. The predicted MET-WRF averaged reflectivity field at the 850-500hPa and 850-750hPa layer as well as the maximum reflectivity between 1000 and 100hPa were tested in this study to find the most suitable layer of model simulated reflectivity in RaINS.

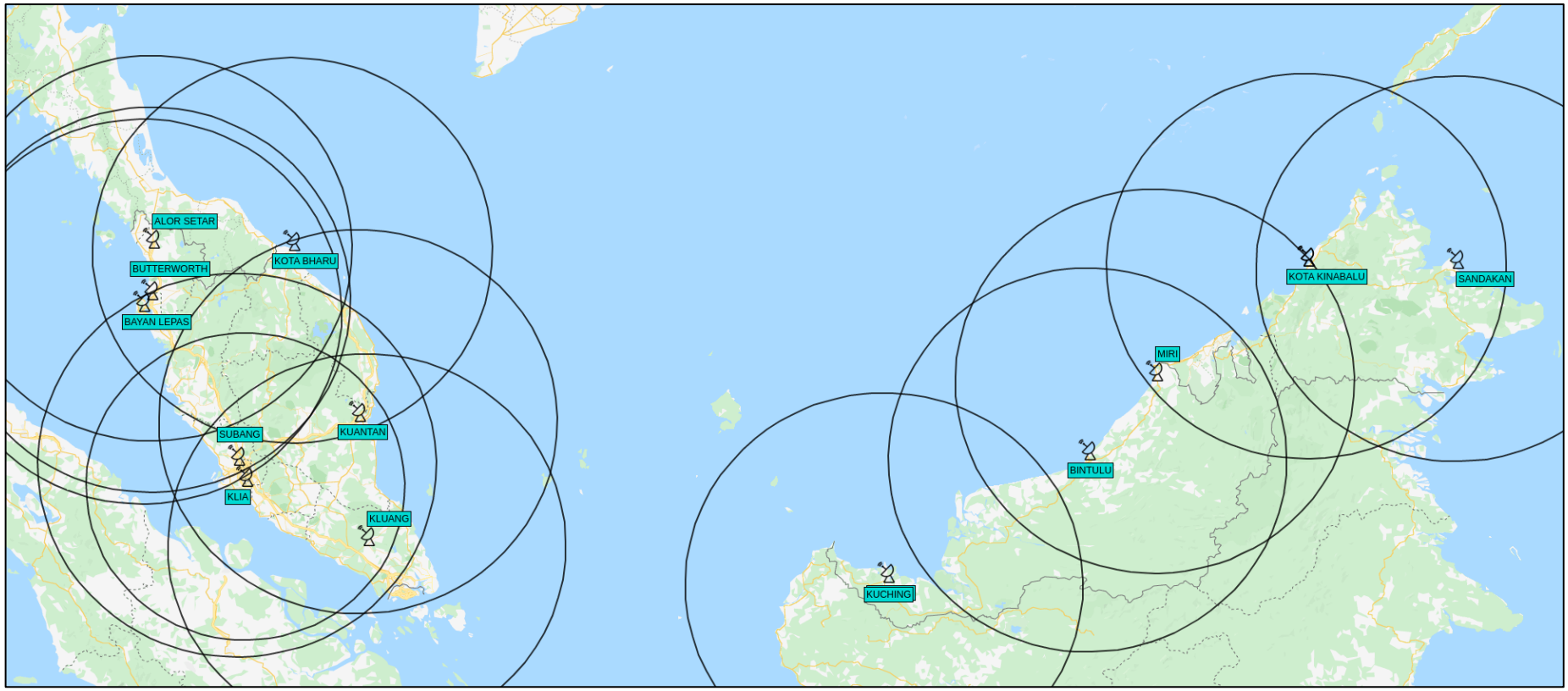


**Figure 1.** Radar coverage in Malaysia.

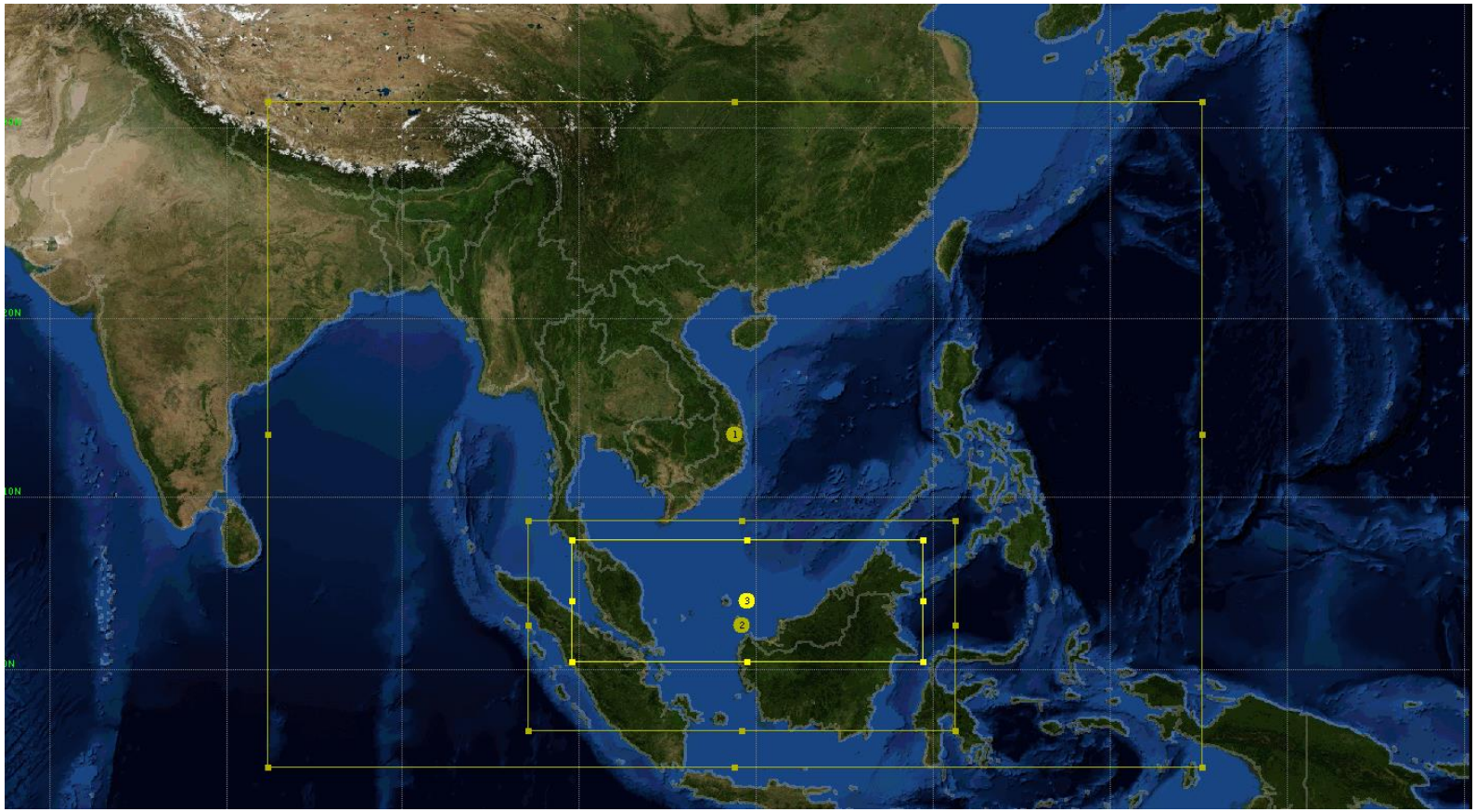

**Figure 2.** Parent domain of MET-WRF at 9km (largest), 3km (d02), and 1km (d01-smallest).

## 3. Methodology

This section begins with an explanation of the optical flow parameters used by the SWIRLS radar extrapolation system in this study. After that, the present configuration of RaINS operationalized by the MMD was described. Finally, the configuration of RaINS tested in this study is described.

### 3.1. Optical flow parameters

This study compares the performance of just one SWIRLS radar velocity [14] which is also used in daily operation, versus the performance of the ensemble average of several SWIRLS radar velocities. The ROVER parameters used in this study were determined through trial experiments using squall-line cases in Malaysia. There are 7 parameters used in the ROVER algorithm to calculate echo motion by optical flow. Five parameters denoted by Lf, Lc, σ, α, and ρ control variational optical flow. Further details regarding the variational optical flow technique used here are available from [18], [19] and [20]. Two other parameters (Zc, and ζ) control image mapping to grayscale using Arc-Tangent Filter [20].

Prior to calculating the echo motion field by optical flow, the radar data are mapped to grayscale images to resolve intense individual echoes and eliminate noise [14,20]. The parameter ζ controls the contrast between radar echoes above and radar echoes below Zc when the radar image is mapped to the new grayscale image. Higher ζ produces sharper contrast while lower ζ reduces contrast. Zc is also known as threshold of significant con-vection while ζ is also known as the sharpness of inflection around Zc. RaINS sets the Zc to be equal to two thirds the maximum radar reflectivity of the current radar image. This scales for all types of radar echoes including relatively less intense radar echoes. For ex-ample, if Zc is fixed at 33dBZ, storms with less intensity than 33dBZ will be filtered too much. Since RaINS is targeted to operate for all weather conditions, Zc is designed to be scaled based on ⅔ (two thirds) of the current maximum radar reflectivity. **Figure 3**. depicts Zc and ζ.

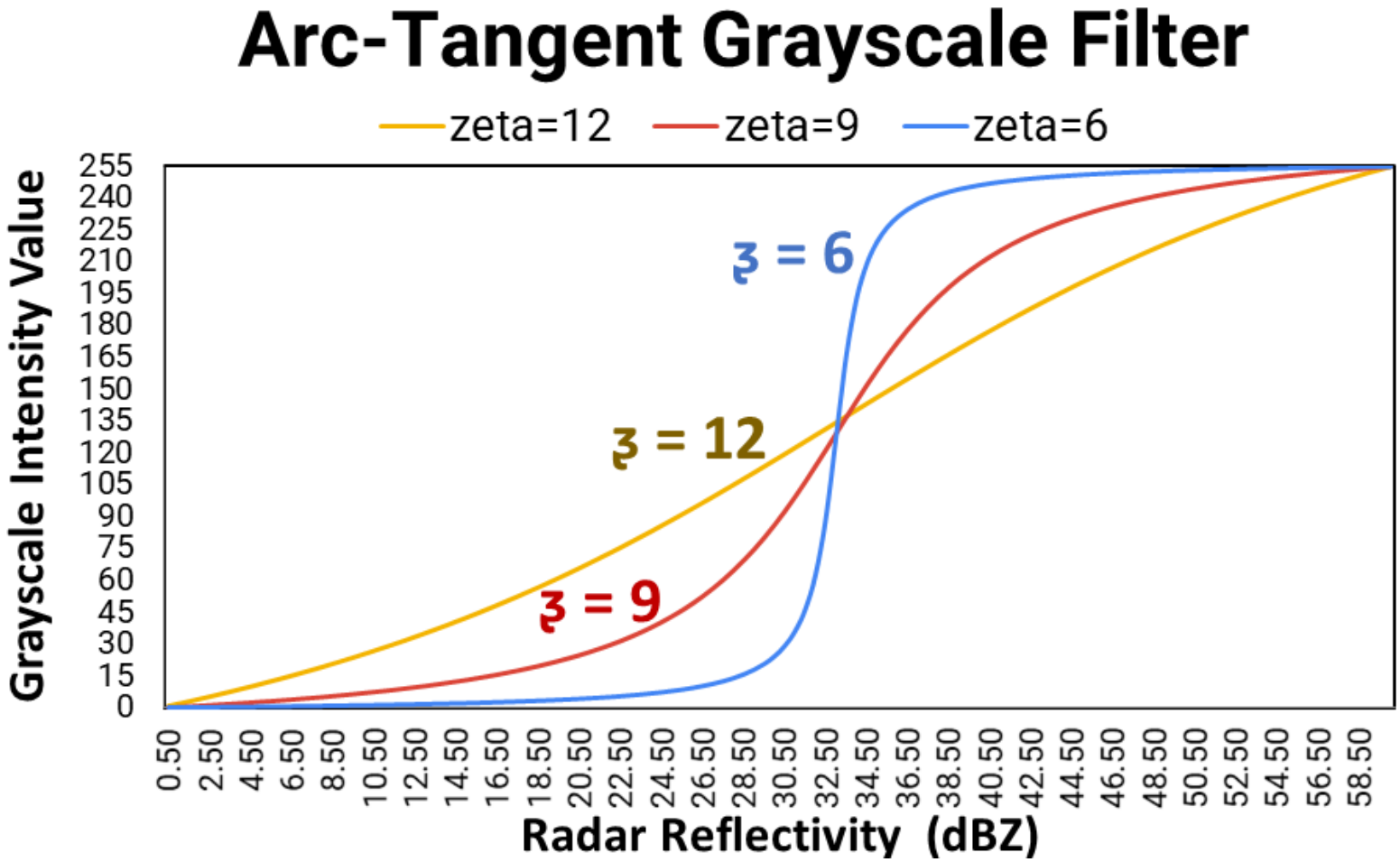


**Figure 3.** The radar reflectivity mapped to grayscale intensity using three separate arc-tangent filters where ζ = 12, 9, and 6 and Zc = 33dBZ.

The radar reflectivity (dBZ) is mapped to grayscale intensity images as depicted in **Figure 3**. The mapping function is mathematically written below:

$$Grayscale = 255 \times \frac{\frac{ATAN(Z-Zc)}{\zeta} - \frac{ATAN(0-Zc)}{\zeta}}{\frac{ATAN(60-Zc)}{\zeta} - \frac{ATAN(0-Zc)}{\zeta}} \quad (1)$$

where Z is the radar reflectivity of the radar image from 0 to 60dBZ mapped to grayscale value from 0 to 255 while Zc is the threshold of significant convection and ζ is the inflection centred at Zc.

After grayscale mapping, the velocity vector field of the radar images is computed through variational optical flow. There are six parameters used namely Lf, Lc, σ, α, and ρ. Lf is the finest spatial scale while Lc is the coarsest spatial scale. [18] used a multigrid approach to speed up optical flow calculation. The solution at the coarsest grid (Lc = 7 pixels) was used as initialization on the next finer grid until the finest grid (Lf = 1 pixel). This multigrid approach allows error reduction by removing high frequency errors on the coarser grid which will otherwise appear as low frequency errors on the finest grid.

Meanwhile, the parameter σ represented the Gaussian convolution for image smoothing [11]. It smooths the image through a low-pass Gaussian convolution filter to remove noise and destabilize other high frequency errors [19]. Moderate pre-smoothing improves optical flow accuracy but too much pre-smoothing may destroy important image information. Subsequently, parameter α is known as the regularization parameter [18]. Larger values of α leads to smoother motion vectors across the radar domain [19]. Parameter ρ is called the Gaussian convolution for local vector field smoothing [11]. Within a neighbourhood of size ρ, the optic flow vector is assumed to be constant [19]. To calculate the optical flow, the following equation is minimized [18]:

$$E(u,v) = \int_{\Omega} \left( w^T J_P(\nabla_3 f) w + \alpha(|\nabla u|^2 + |\nabla v|^2) \right) \mathrm{dxdy} \quad (2)$$

where E(u,v) is the energy function to be minimized, Ω is the entire domain space, w(x,y) = ( u(x,y), v(x,y), 1 )$^T$ is the displacement, ∇u is the spatial gradient ($u_x$ , $u_y$) $^T$, u and v are zonal and meridional components of velocity, and $\nabla_3 f$ denotes the spatiotemporal gradient of grayscale intensity ($I_x$ , $I_y$, $I_t$ ).

### 3.2. Operational RaINS Configuration

Radar velocity flow field to be used in SWIRLS was calculated using a single set of parameters (Zc, ζ, $L_f$, $L_c$, σ, α, and ρ) that is described in **Table 1.** Subsequently, the maximum NWP reflectivity between 1000hPa and 100hPa was blended with the SWIRLS output with the following equation:

$$RaINS(T, dBZ) = w(T) * NWP(T, dBZ) + \big(1 - w(T)\big) * SWIRLS(T, dBZ) \quad (3)$$

where RaINS (T, dBZ) is the final nowcast output in units of reflectivity, SWIRLS (T, dBZ) is the output of SWIRLS extrapolated radar reflectivity in units of reflectivity, and w(T) is the time (T) varying hyperbolic tangent weighting function denoted by the following equation:

$$w(T) = \alpha + \varepsilon \times (1 + tanh\{\gamma \times [T - 9]\}) \quad (4)$$

where ε controls the rate at which w(T) rises (gradient), γ is a constant equal to 0.24, and T is the nowcast lead time in minutes. Equation 4 is just the simplified form of [8] and [13] where α is equals to zero. In this study, a single hyperbolic tangent function denoted by $w_1(T \mid \varepsilon = 0.50)$ was evaluated.

In operational RaINS, one (1) hyperbolic tangent function was selected out of 13 hyperbolic tangent functions $w_i$ ($T \mid \varepsilon_i$ = 0.51, 0.46, 0.42, 0.39, 0.36, 0.32, 0.28, 0.25, 0.21, 0.17, 0.14, 0.10, 0.07, and 0.00). The hyperbolic tangent function that minimizes the following equation (6) is selected.

$$Error_i(dBZ) = \sum_{T=0}^{-180} \Big(RADAR_T(dBZ) - RaINS_{T,i}(dBZ)\Big)^2 \quad (5)$$

$$RaINS_{T,i}(dBZ) = w_i(T) * NWP(dBZ) + \big(1 - w_i(T)\big) * SWIRLS(dBZ) \quad (6)$$

$$w_i(T) = \alpha + \epsilon_i \times (1 + tanh\{\gamma \times [T - 9]\}) \quad (7)$$

where weight $w_i(T)$ which minimizes $Error_i$ (dBZ) is chosen. The variable $Error_i$ (dBZ) is the sum of the square difference between observed radar reflectivity RADAR (dBZ) at time T with RaINS nowcast using weight i at time T. Meanwhile, T is the past forecast or hindcast between now (T=0) and T=-10, -20, ..., -170, -180 minutes. This scheme introduces persistence into the RaINS nowcast. This paper compares the single constant

weight scheme (known as constant weighing in this study) with the operational weighting scheme that introduces persistence (called persistence weighing in this study). **Figure 4**. depicts the single weight used in RaINS, while **Figure 5** depicts the operational weighting scheme with persistence introduced in this study. **Table 2** summarizes the differences between RaINS in operational mode versus RaINS tested in this study.

**Table 1.** Parameter values for ensemble average flow and for single parameter flow.

| **Parameters** | **Ensemble Average Flow** | **Single Parameter Flow** |
|---|---|---|
| $Z_c$ (Threshold for significant convection) | 2/3 maximum reflectivity | 2/3 maximum reflectivity |
| $\zeta$ | 6, 9, and 12 | 12 |
| $L_f$ (Finest spatial scale) | 1 | 1 |
| $L_c$ (Coarsest spatial scale) | 7 | 9 |
| $\sigma$ (Gaussian convolution for image smoothing) | 18, 24 and 40 | 40 |
| $\alpha$ (Regularization parameter) | 1000 | 1000 |
| $\rho$ (Gaussian convolution for local scale smoothing) | 3, 4 and 9 | 9 |

**Table 2.** RaINS in operational mode (middle column) and RaINS studied (right column).

| | **RaINS Operational** | **RaINS in this study** |
|---|---|---|
| SWIRLS radar velocity flow | Average of ensemble flow (**Table 1** column 2) | Single member flow (**Table 1** column 3) |
| Hyperbolic tangent weights blending SWIRLS & NWP | One weight selected out of several weights based on past radar observation (**Figure 2**) | One single weight (**Figure 3**) |
| NWP Reflectivity Level | Maximum reflectivity between 1000hPa to 100hPa | Average 850-750hPa<br>Average 850-500hPa |

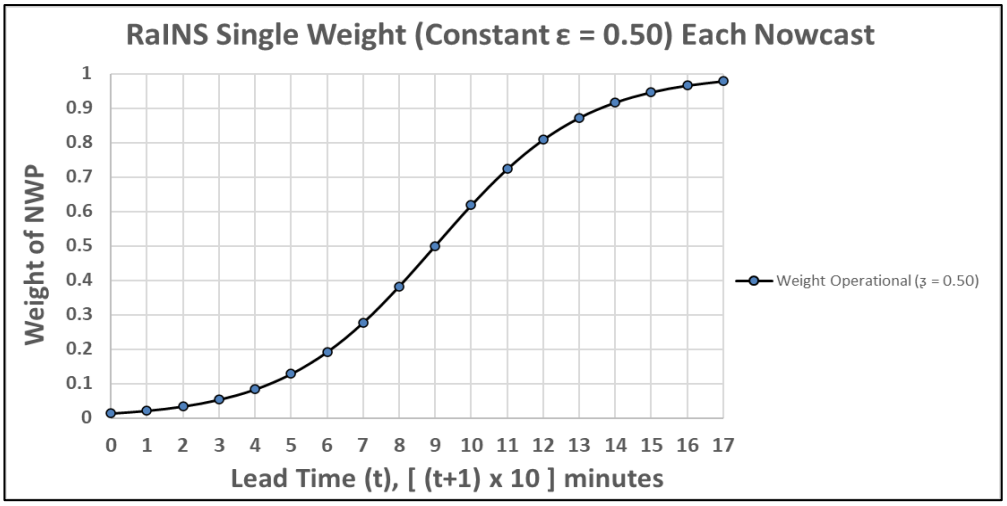


**Figure 4.** Single hyperbolic tangent curve tested in this study. It resembles the first weight of the 13 ensembles of weights in Figure 5.

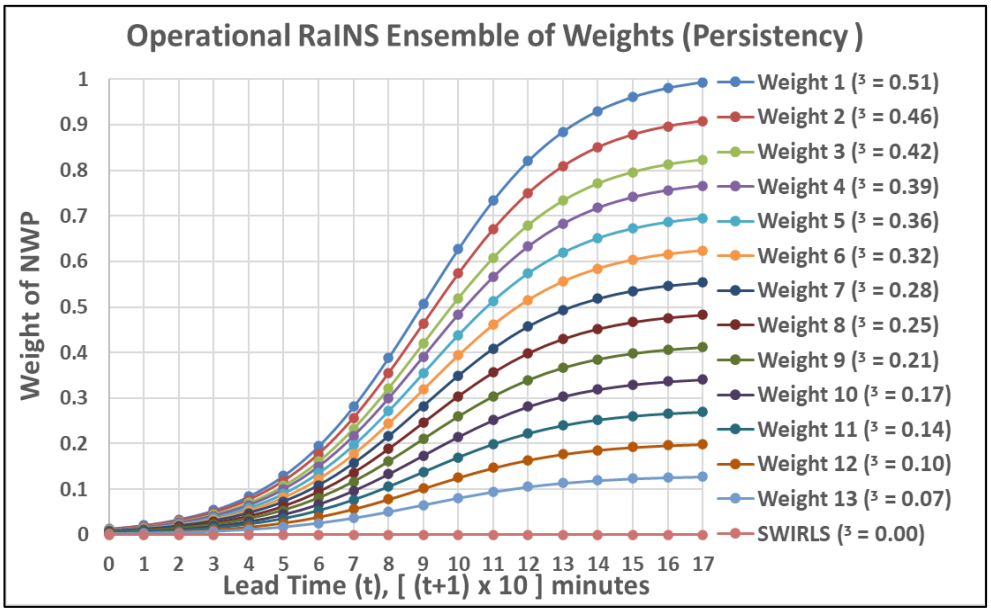


**Figure 5.** Operational weighting scheme. Series of weights of which one is selected to blend SWIRLS-NWP based on past radar data. This introduces persistence in RaINS nowcast.

## 4. Results and Discussion

The performance of RaINS was evaluated during two (2) significant cyclonic vortex events. The time of verification are summarized in **Table 3** while the domains of verification are depicted in **Figures 6** and **7**. Each radar observation and corresponding RaINS nowcast are paired together and mapped to the same domain (**Figure 2; 1km domain).** The resolution of radar observation and nowcast are 1km. The nowcasts are evaluated by defining rainfall as events exceeding 10dBZ. This threshold is arbitrarily chosen to evaluate and identify the best configuration of RaINS. RaINS is objectively evaluated by matching each nowcast grid and nowcast time with corresponding radar grid and radar time within the verification domain (**Figures 6** and **7**). The results of the match are depicted in the Contingency Table (**Table 4**). The Probability of Detection (POD) and False Alarm Ratio (FAR) are depicted by **Equation 8.**

**Table 3.** The date and time for each stage of the storm that are used to verify RaINS.

| | **Date of Event / Time of Storm Stage** | **04 - 05 November 2017** | **22-23 December 2017** |
|---|---|---|---|
| **Stage of the Storm** | **Initial** | 04:00 - 06:50 | 18:00 - 21:00 |
| | **Mature** | 13:00 - 15:50 | 21:10 - 01:00 |
| | **Decaying** | 22:00 - 00:50 | 01:10 - 05:00 |

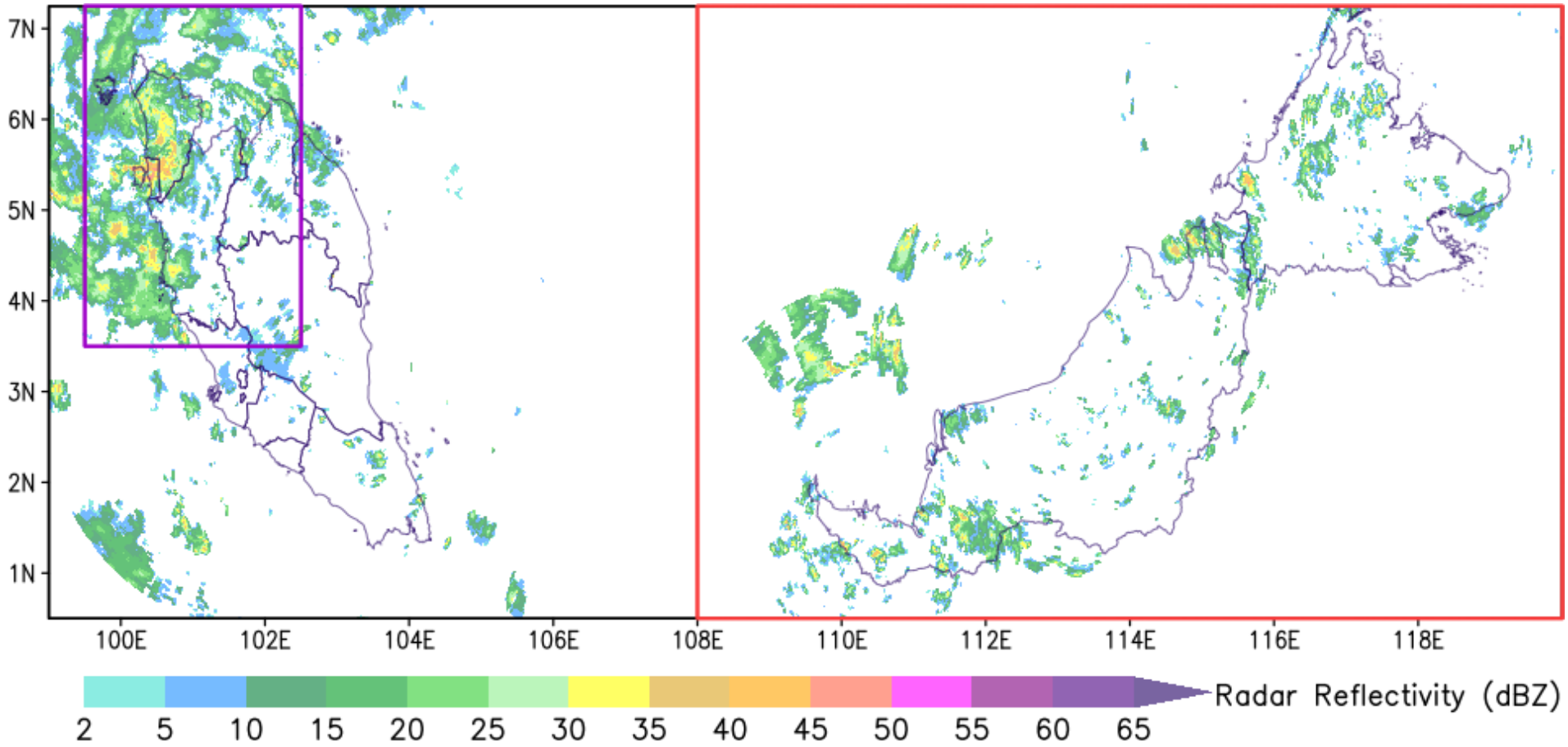


**Figure 6.** The domain inside the cyclonic vortex (purple) and outside the vortex (red).

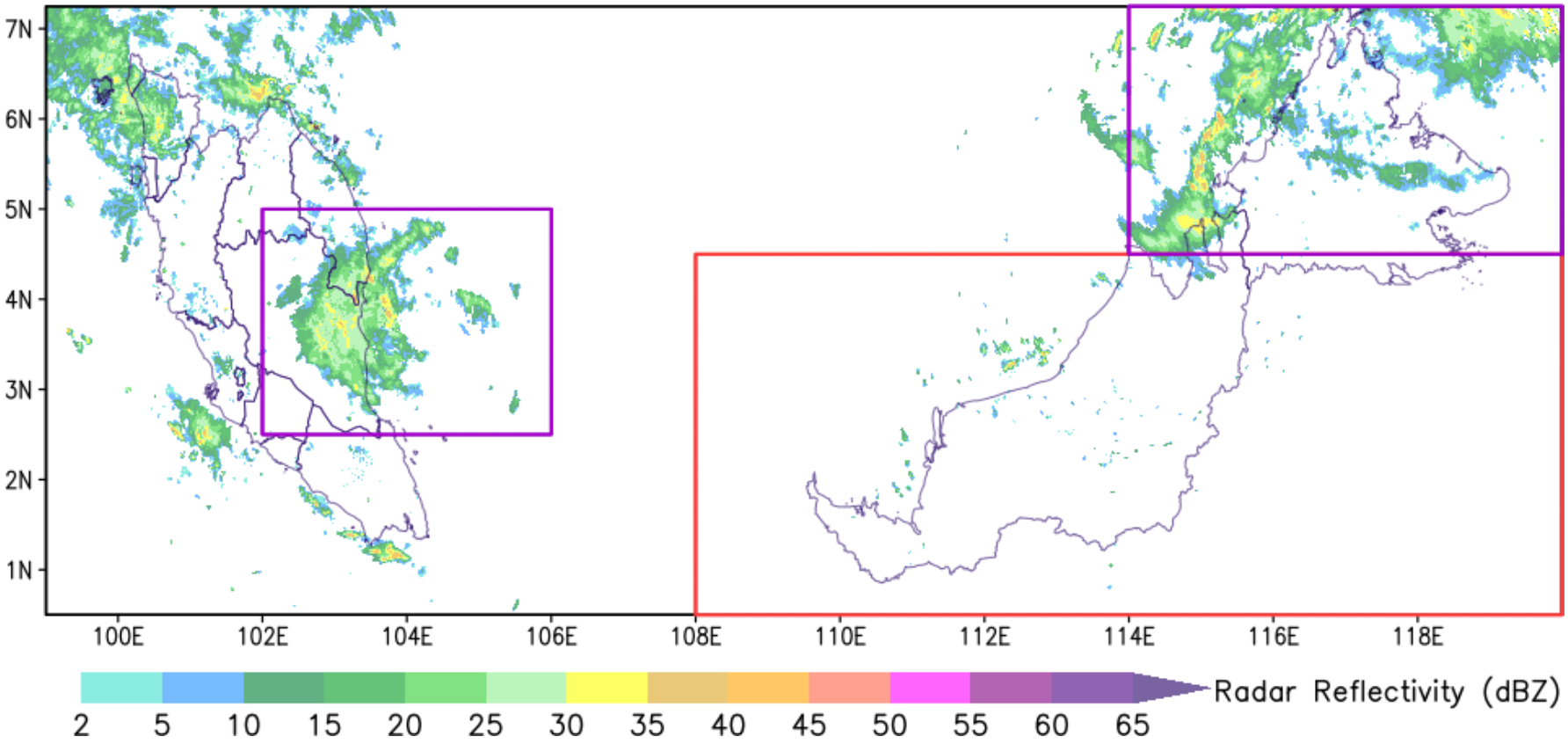


**Figure 7.** The domain inside the cyclonic vortex (purple) and outside the vortex (red).

**Table 4.** Contingency table calculated for each grid point at each time.

| Category | | Radar Observation | |
|---|---|---|---|
| | | **Yes (>= 10 dBZ)** | **No (< 10dBZ)** |
| **Nowcast** | **Yes (>= 10 dBZ)** | Hits | False Alarms |
| | **No (< 10dBZ)** | Miss | Correct Negatives |

$$POD = \frac{Hits}{Hits + Miss}; FAR = \frac{FalseAlarms}{FalseAlarms + Hits} \quad (8)$$

**Figures 8** and **9** depict the POD and FAR of RaINS using model simulated maximum reflectivity, 850-750hPa average reflectivity, and 850-500hPa average reflectivity aggregated over both cyclonic events in this study and areas inside and outside the storm. The maximum reflectivity gave higher POD than averaged reflectivity with relatively negligible change in FAR. This may be explained as follows.

During the mature stage, the cloud base is lowered in the updraft region. The mechanism is explained as follows. The updraft entrains air from outside the cloud with moist rain-cooled air just below the rainy portion of the cloud. The air in the updraft region is cooled by evaporation of liquid water from rainfall and adiabatic expansion from vertical ascent [21]. Addition of moisture from rainfall regions of the cloud along with adiabatic cooling and steeper lapse read [21] leads to lower air parcel temperature and increased relative humidity. This lowers the lifted condensation level [22].

On the other hand, in both the mature and dissipating storm stage, cloud height top expands from 15,000 feet in the initial stage to 30,000 feet and 40,000 feet respectively [21]. Therefore, the maximum reflectivity from 1000hPa to 100hPa may better capture the expansion of cloud height by using a deeper atmospheric depth compared to a narrow atmospheric depth represented by the average reflectivity fields of 850-500hPa and 850-750hPa layers.

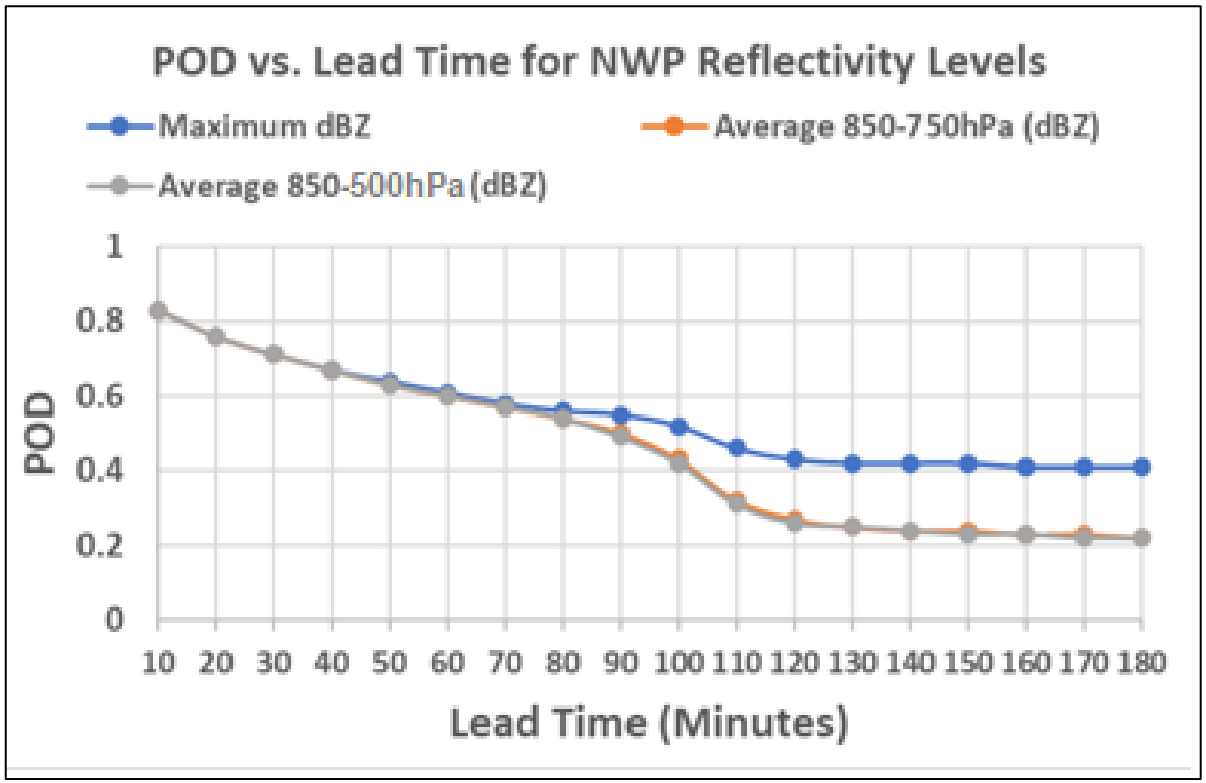


**Figure 8**. POD of RaINS for NWP reflectivity levels

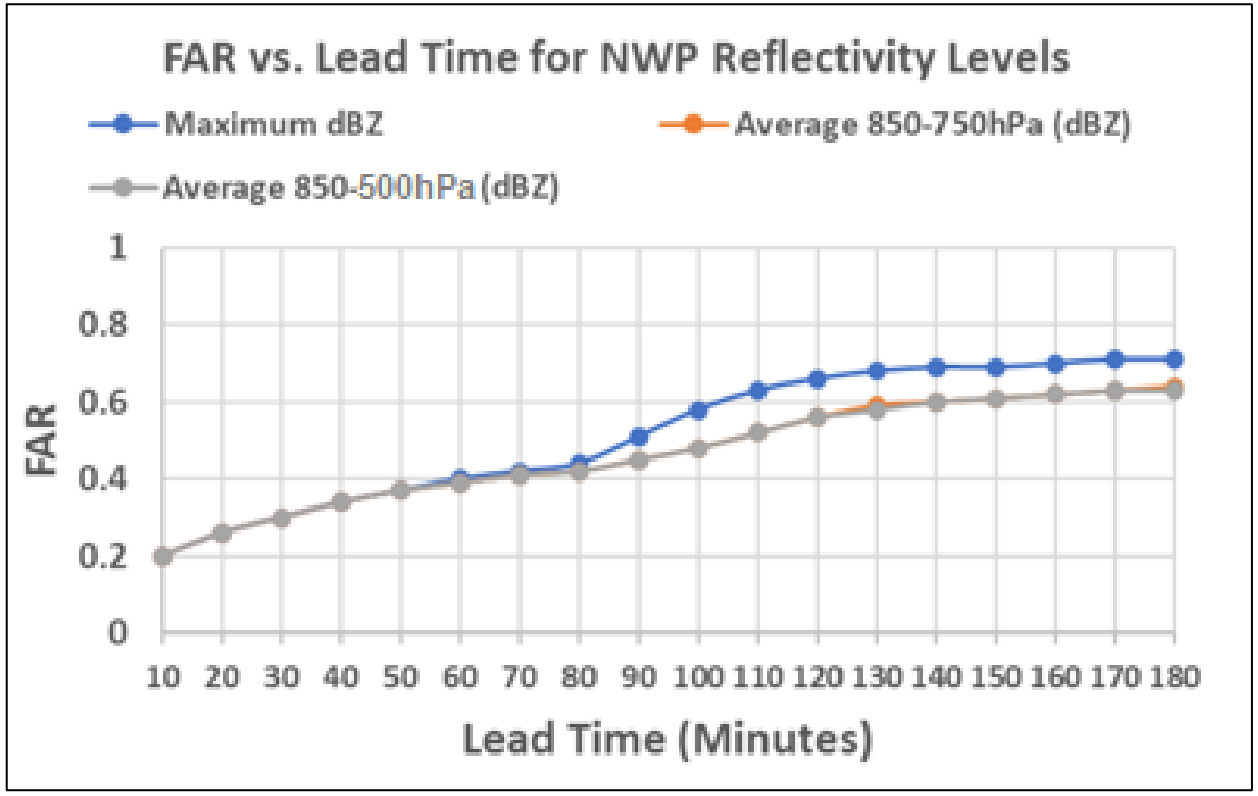


**Figure 9**. FAR of RaINS for NWP reflectivity levels.

Meanwhile, the RaINS configuration which blends radar extrapolation using persistence weighing is more skilful than RaINS configuration using constant weight. This is indicated by **Figures 10** which indicate higher POD and lower FAR of persistence weighing compared to fixed weight. The persistence term could have suppressed rainfall overestimation in RaINS. This persistence was created through the selection of a nowcast weight that most resembles radar observation three hours ago. Inclusion of past radar observation in RaINS in the form of the persistence term was considered a substitute for the absence of real time radar data assimilation into the NWP model.

On the other hand, SWIRLS radar velocity flow computed as an ensemble average of several parameters ($Z_c$, $\zeta$, $L_f$, $L_c$, $\sigma$, $\alpha$, and $\rho$) outperforms SWIRLS radar velocity flow computed using just a single member. **Figure 11**. showed that the ensemble average flow has marginally higher POD than single member flow with FAR nearly constant. This happens because each geographical setting has its own optimal parameters [11].

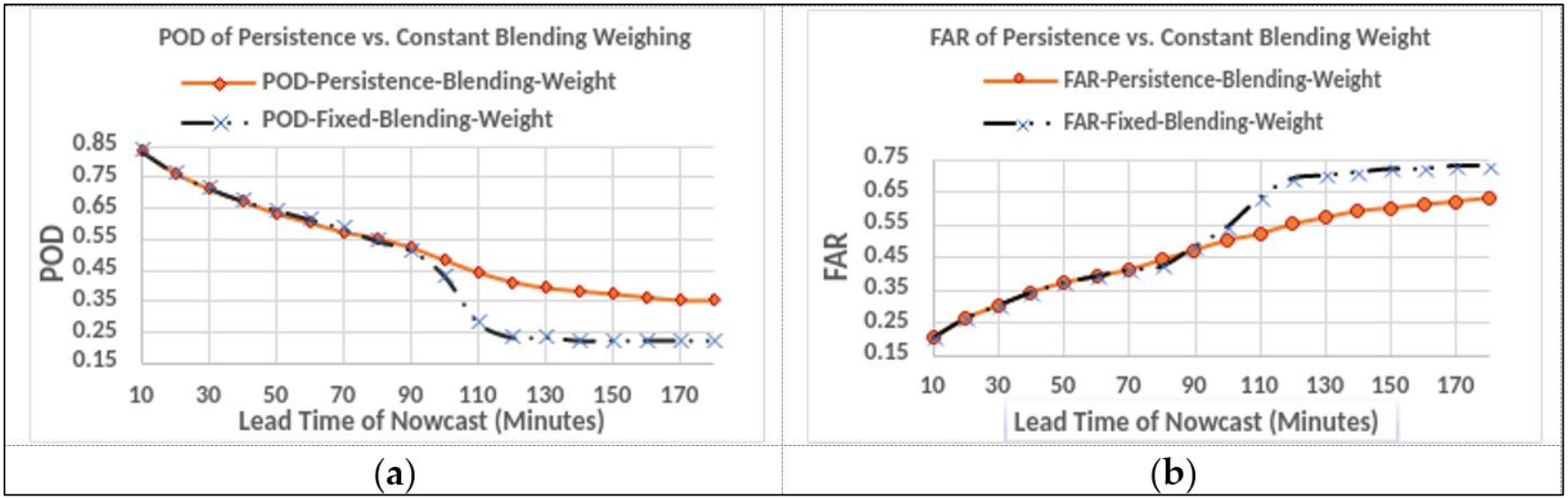


**Figure 10.** POD (FAR) of persistence weight scheme versus constant weight scheme in left (right) figure.

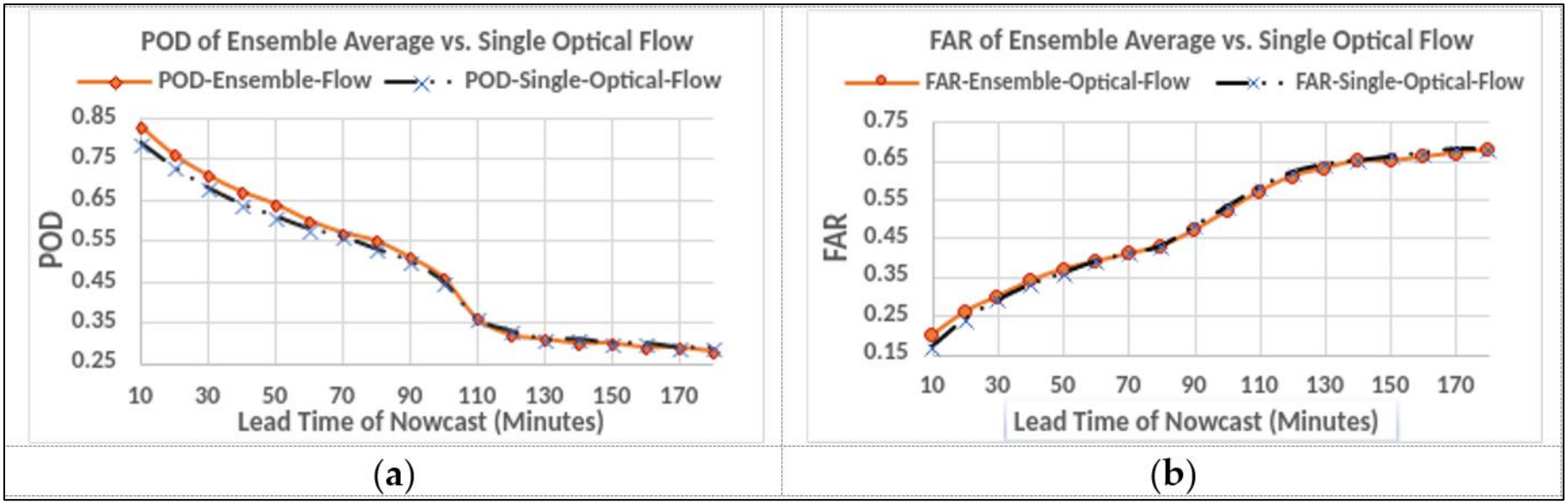


**Figure 11**. POD(FAR) of ensemble average optical flow vs. single member optical flow in left (right) figure.

Nowcasting over a large domain involves multiple geographical settings. Therefore, averaging multiple parameters is a computationally cheap method of improving the skill score over a large domain. Additionally, the averaging process cancels off random errors that may be present in each individual ensemble member. RaINS using persistence weighing in conjunction with the ensemble average optical flow outperforms RaINS with fixed weight in conjunction with single optical flow. **Figures 12** and **13** showed that RaINS has higher POD and lower FAR at all lead times, especially after 90 minutes.

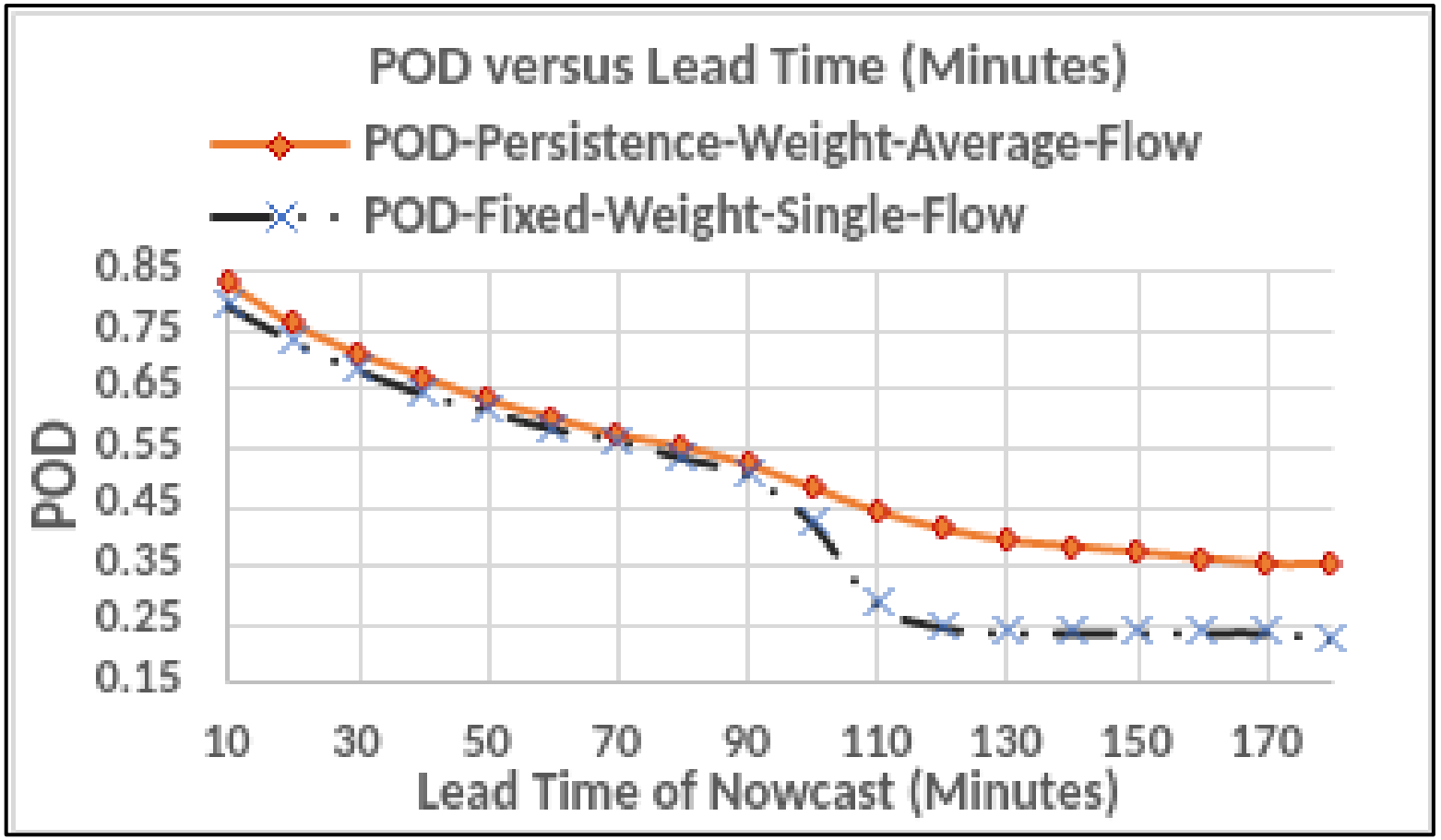


**Figure 12**. POD vs. lead time; Persistence-Weight-Average-Flow vs. Fixed-Weight-Single-Flow.

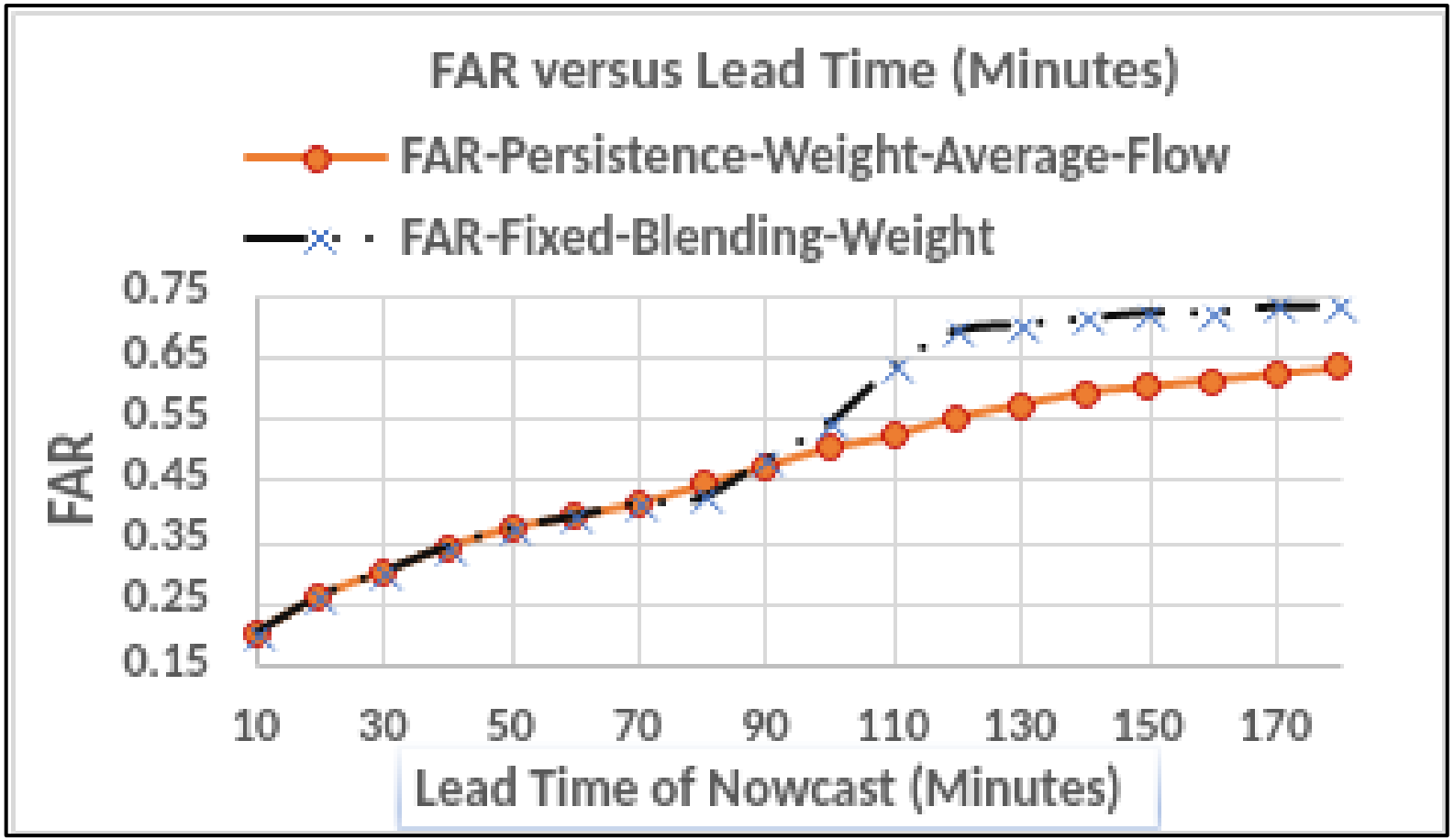


**Figure 13**. FAR vs. lead time; Persistence-Weight-Average-Flow vs. Fixed-Weight-Single-Flow.

The useful lead time is defined as POD greater than FAR. This implies that the nowcast is more likely to hit than being a false alarm within a given lead time. Additionally, useful lead time is also defined as POD greater than 0.5. This means that the nowcast is more likely to hit rather than miss. Finally, useful lead time is given by FAR less than 0.5. This means that the probability of the nowcast being a false alarm is less than 0.5. Rainfall is defined by grid points having a value exceeding 10dBZ. Calculations of POD and FAR of RaINS indicate that RaINS has a useful lead time of 100 minutes for regions inside the storm or cyclonic vortex. On the other hand, RaINS has a reduced useful lead time of just 50 minutes for convective storms outside of the cyclonic vortex. These convective storms were shorter-lived, lasting less than 3 hours with rapid growth and decay in the order of minutes compared to the main cyclonic circulation. **Figures 14** and **15** indicated that the skill of RaINS is reduced for convective storms outside the storm compared to the main storm inside the circulation.

This reduction in skill was consistent with the work of [23,24] who both used WRF. [23] reported only one out of four local thunderstorms near Darwin, Australia was detected but [24] in contrast was able to accurately capture rainfall intensity and spatial distribution for cyclone Phailin. The drop in accuracy between large scale cyclonic circulations and smaller scale local thunderstorms occur because initiation and development of localized convective systems are stochastic in nature that could not be precisely predicted but may be analyzed statistically. To increase the NWP accuracy, [23] assimilated radiosonde data at a 3 hourly interval with WRF model that is initialized 10 hours before the local thunderstorm began. It was reported that four out of four local thunderstorms were accurately simulated by the WRF model. Hence, observational nudging at near-real time may be required to increase accuracy of nowcasts in local thunderstorms away from the main cyclonic circulation.

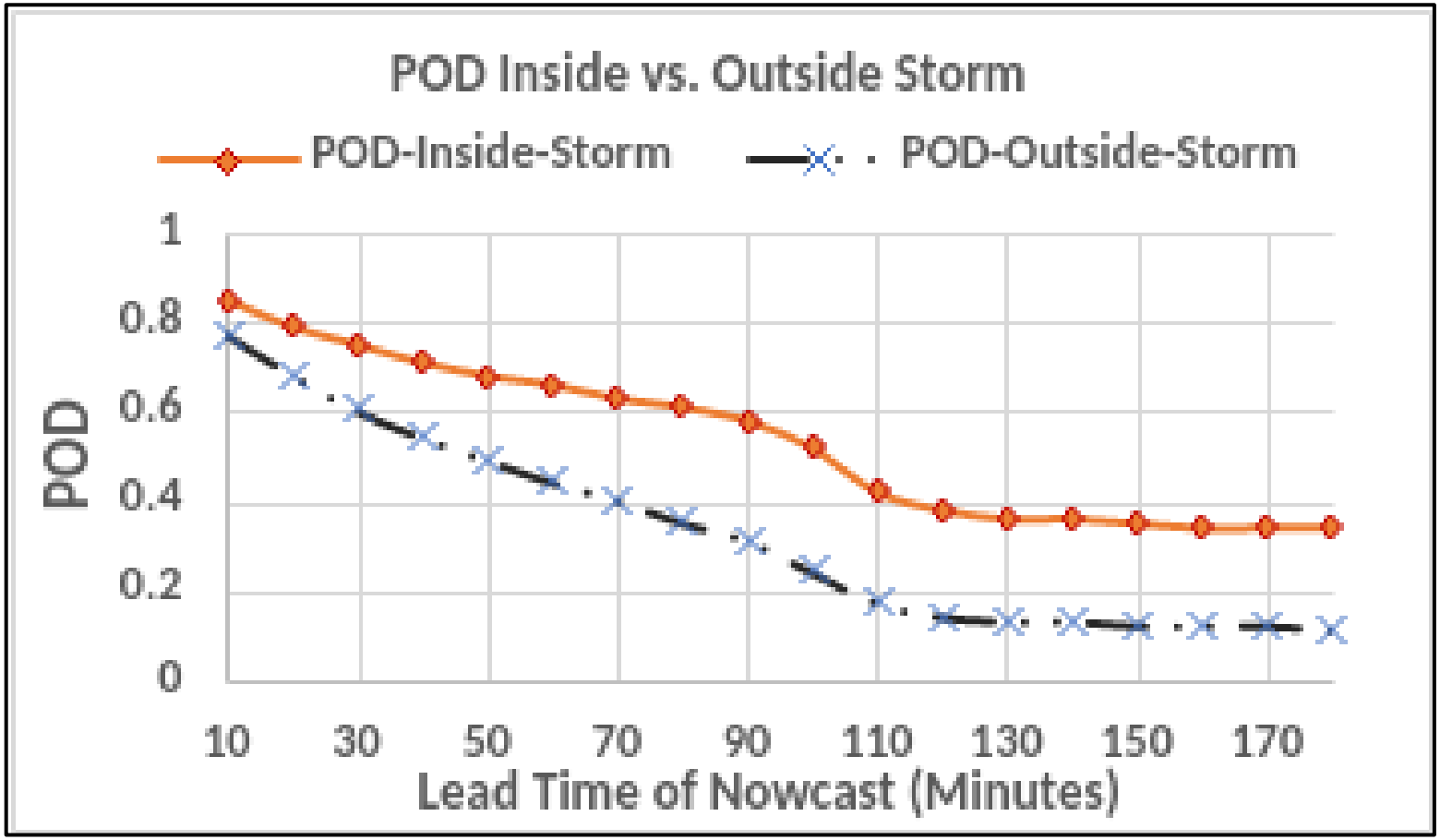


**Figure 14.** POD vs. lead time; inside compared to outside the storm.

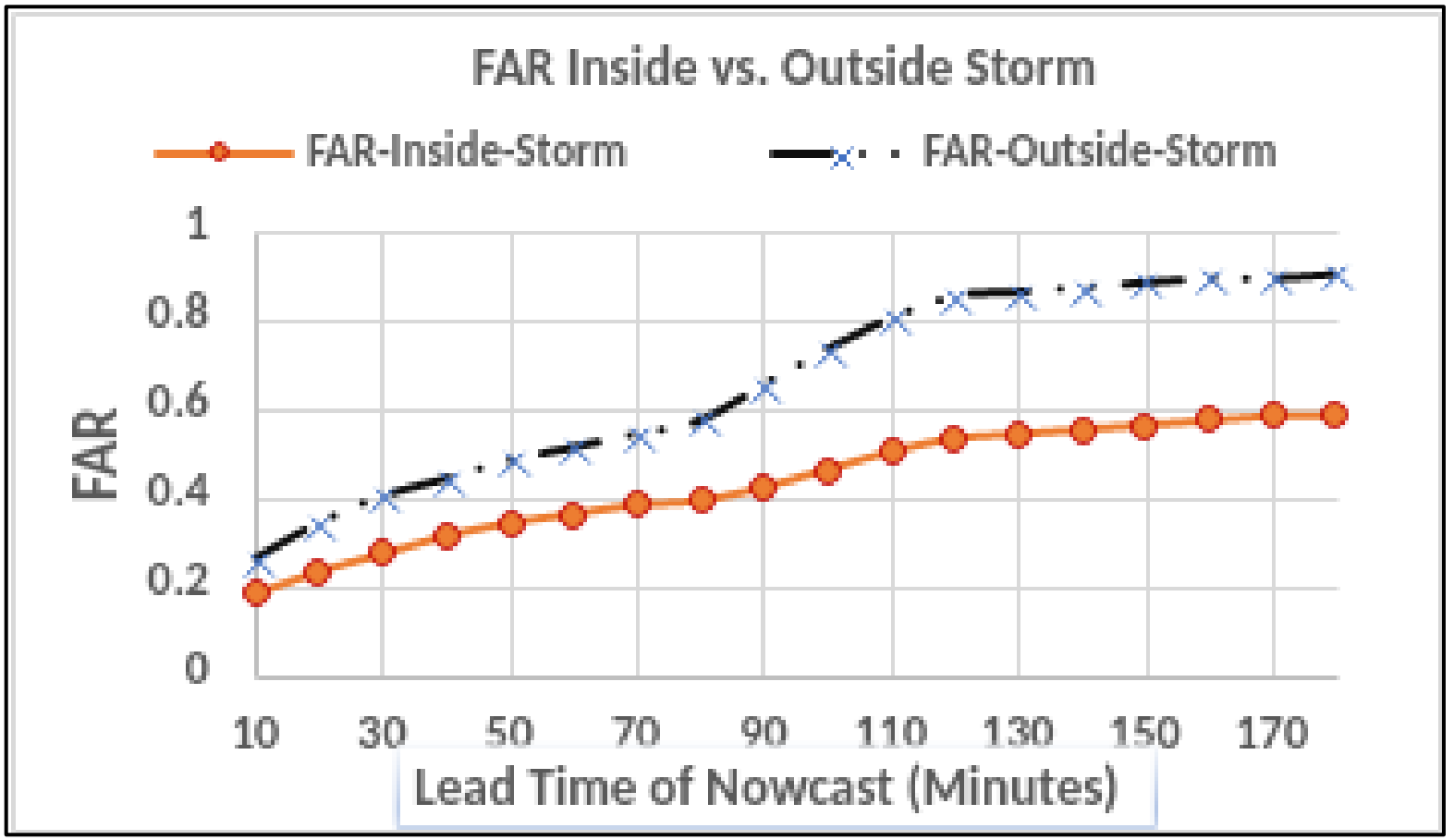


**Figure 15**. FAR vs. lead time; inside compared to outside the storm.

In a nutshell, using the multiple weight configuration in conjunction with maximum NWP reflectivity calculated between 1000hPa to 100hPa blended with an ensemble average SWIRLS-QPF optical flow yielded the highest accuracy. This summary was true for storms in the cyclonic circulation and local storms away from the cyclonic circulation.

## 5. Conclusion

The development and system design of RaINS are introduced in this paper. Fine-tuning of RaINS has been conducted using two cyclonic circulation cases for storms both inside the circulation itself and for convective scale storms away from the circulation. Evaluation of RaINS performance using POD and FAR revealed that maximum 1000hPa to 100hPa NWP reflectivity gives the highest skill level. RaINS is further improved when the NWP to radar extrapolation weight is selected by considering persistence based on past radar observations. Finally, a further increase in skill is noted when the average motion vector of radar extrapolation consists of the ensemble average of multiple parameters.

The accuracy of the radar extrapolation may be improved by adopting deep learning precipitation nowcasting. As noted in [25], several deep learning nowcast models such as the Trajectory Gated-Recurrent Unit (TrajGRU) have been developed that can outperform the optical flow method for heavy rain. Hence, implementation of deep learning methods in the radar nowcast component in RaINS will be investigated in the future to compare its accuracy alongside with the SWIRLS optical flow method used in this study.

This study also reveals a limitation of RaINS that needs to be addressed. RaINS is skillful in large scale cyclonic storms but suffers from a severe drop in skill for smaller scale convective storms. Further investigation should be performed in assimilating near-real time observation to NWP forecast to predict the rapid evolution of smaller-scale convection.

## 6. Acknowledgement

The authors would like to acknowledge Ms. Fauziana binti Ahmad from the Radar and Satellite Division for providing the radar data, and Ms. Wan Maisarah binti Wan Ibadullah for provision of MET-WRF NWP data for the case studies.

**References**


1. Johnson, J.T., et al. (1998). The storm cell identification and tracking algorithm: An enhanced WSR-88D algorithm. *Weather and forecasting, 13(2),* 263-276. https://doi.org/10.1175/1520-0434(1998)013<0263:TSCIAT>2.0.CO;2
2. Dixon, M., & Wiener, G. (1993). TITAN: Thunderstorm identification, tracking, analysis, and nowcasting - A radar-based methodology. *Journal of atmospheric and oceanic technology, 10 (6),* 785-797. https://doi.org/10.1175/1520-0426(1993)010<0785:TTITAA>2.0.CO;2
3. Hering, A.M., et al. (2004, September). Nowcasting thunderstorms in the Alpine region using a radar based adaptive thresholding scheme. In *Proceedings of ERAD* (Vol. 1, No. 6).
4. Chornoboy, E.S., Matlin, A.M., and Morgan, J.P. (1994). Automated Storm Tracking for Terminal Air Traffic Control. *The Lincoln Laboratory Journal.* 7(2) pp 427 - 448.
5. Rinehart, R.E., and Garvey, E.T. (1978). Three-dimensional storm motion detection by conventional weather radar. *Nature, 273 (5660)* pp 287-289.
6. Wong, M.C., Wong, W.K., and Lai, E.S. (2006). From SWIRLS to RAPIDS: Nowcast applications development in Hong Kong. *In PWS Workshop on Warning of Real-Time Hazards by Using Nowcasting Technology, Sydney, Australia, 9-13 October 2006.*
7. Li, L., W. Schmid., and Joss, J. (1995). Nowcasting of motion and growth precipitation with radar over a complex orography. *Journal of applied meteorology and climatology, 34(6)* pp 1286 - 1300.
8. Wang et al., (2015). Improvement of forecast skill for severe weather by merging radar-based extrapolation and storm-scale NWP corrected forecast. *Atmospheric Research,* 154, pp 14-24. https://doi.org/10.1016/j.atmosres.2014.10.021.
9. Wong et al. (2009). Towards the blending of NWP with nowcast - Operation experience in B08FDP. In the WMO *symposium on Nowcasting Volume 30,* p. 4.
10. Cheung, P., Li, P.W., and Wong, W.K. (2015). Blending of extrapolated radar reflectivity with simulated reflectivity from NWP for a seamless significant convection forecast up to 6 hours. *Hong Kong Observatory Reprint* **1182**.
11. Woo, W. C., & Wong, W. K. (2017). Operational application of optical flow techniques to radar-based rainfall nowcasting. *Atmosphere*, *8*(3), 48. https://doi.org/10.3390/atmos8030048.

12. Tong Y.F., and Lai, S.T., (2006). Applications of NWP and Nowcasting Techniques for the Warning of Rainstorms and Landslips. *Hong Kong Observatory Reprint* **663.**
13. Li, P.W., Wong, W.K., and Lai, S.T., (2005). RAPIDS - A new rainstorm nowcasting system in Hong Kong. In *Proceeding, WWRP Symposium on Nowcasting and Very Short Range Forecasting* (pp. 7-17).
14. Diong D.J., et al. (2018). Analysis of the Cyclonic Vortex and Evaluation of the Performance of the Radar Integrated Nowcasting System (RaINS) during the Heavy Rainfall Episode which caused Flooding in Penang, Malaysia on 5 November 2017. *Tropical Cyclone Research and Review*, 7(4) pp 217 - 229. https://doi.org/10.6057/2018TCRR04.03
15. Roy et al. (2010). Doppler weather radar based nowcasting of cyclone Ogni. *Journal of earth system science*, *119*(2), 183-199. https://doi.org/10.1007/s12040-010-0016-7
16. Ahmad., F., et al. (2018). Comparison of CAPPI Height 2km and 1km during Northeast Monsoon. *MET Malaysia Research Publication 2018 (1).*
17. Skamarock et al. (2008). A description of the Advanced Research WRF version 3. NCAR Technical note-475+ STR. p 113.
18. Bruhn, A., Weickert, J., Feddern, C., Kohlberger, T., & Schnörr, C. (2003, August). Real-time optic flow computation with variational methods. In *International Conference on Computer Analysis of Images and Patterns* (pp. 222-229). Springer, Berlin, Heidelberg. https://doi.org/10.1007/978-3-540-45179-2_28.
19. Bruhn, A., Weickert, J., & Schnörr, C. (2002, September). Combining the advantages of local and global optic flow methods. In *Joint Pattern Recognition Symposium* (pp. 454-462). Springer, Berlin, Heidelberg. https://doi.org/10.1007/3-540-45783-6_55
20. Cheung, P., & Yeung, H. Y. (2012, August). Application of optical-flow technique to significant convection nowcast for terminal areas in Hong Kong. In *The 3rd WMO International Symposium on Nowcasting and Very Short-Range Forecasting (WSN12)* (pp. 6-10).
21. Byers, H.R. and Braham, R.R. (1948). Thunderstorm structure and circulation. *Journal of Atmospheric Sciences,* 5(3), 71-86. https://doi.org/10.1175/1520-0469(1948)005%3C0071:TSAC%3E2.0.CO;2
22. Lawrence, M. G. (2005). The relationship between relative humidity and the dewpoint temperature in moist air: A simple conversion and applications. *Bulletin of*

*the American Meteorological Society*, *86*(2), 225-234. https://doi.org/10.1175/BAMS-86-2-225

23. Zhu, M., Connolly, P., Vaughan, G., Choularton, T., & May, P. T. (2013). Numerical simulation of tropical island thunderstorms (Hectors) during the ACTIVE campaign. *Meteorological Applications*, *20*(3), 357-370. https://doi.org/10.1002/met.1295
24. Mahala, B. K., Mohanty, P. K., & Nayak, B. K. (2015). Impact of microphysics schemes in the simulation of cyclone Phailinusing (?) WRF model. *Procedia Engineering*, *116*, 655-662. https://doi.org/10.1016/j.proeng.2015.08.342
25. Shi, X., Gao, Z., Lausen, L., Wang, H., Yeung, D. Y., Wong, W. K., & Woo, W. C. (2017). Deep learning for precipitation nowcasting: A benchmark and a new model. *arXiv preprint arXiv:1706.03458*.

**MALAYSIAN METEOROLOGICAL DEPARTMENT**
**JALAN SULTAN**
**46667 PETALING JAYA**
**SELANGOR DARUL EHSAN**
**Tel : 603-79678000**
**Fax : 603-79550964**
**www.met.gov.my**

ISBN 978-967-2327-17-2